Electrochemical impedance spectroscopy of Ba2In2O5: effect of porosity, grain size, dopant, atmosphere and temperature

Jankovic, Jasna; Wilkinson, David P.; Hui, Rob

Publisher's version / Version de l'éditeur:
https://doi.org/10.1149/2.022202jes
Journal of the Electrochemical Society, 159, 2, pp. B109-B120, 2011-12-15

Journal of The Electrochemical Society, **159** (2) B109-B120 (2012)
0013-4651/2012/159(2)/B109/12/$28.00 © The Electrochemical Society

Electrochemical Impedance Spectroscopy of $Ba_2In_2O_5$: Effect of Porosity, Grain Size, Dopant, Atmosphere and Temperature

Jasna Jankovic,[a,b,*,z] David P. Wilkinson,[a,b,,z] and Rob Hui[b]**

[a]*Department of Chemical and Biological Engineering, University of British Columbia, Vancouver, British Columbia V6T 1Z4, Canada*
[b]*Institute for Fuel Cell Innovation, National Research Council Canada, Vancouver, British Columbia V6T 1W5, Canada*

Electrochemical impedance spectroscopy was used to investigate the electrical properties of $Ba_2In_2O_5$ and the effect of porosity, dopant (Ce), atmosphere, temperature, and grain size on these properties. The effect of dopant was investigated by comparing the results of undoped $Ba_2In_2O_5$ samples to Ce-doped $Ba_2In_2O_5$ samples. Effect of grain size for both compositions was studied by comparing the samples made by the glycine-nitrate method, which resulted in smaller grain sizes, and the samples made by the solid-state process, which resulted in larger grain sizes. Porosity effects were determined by testing the samples with different porosities between 20% and 50%. All samples were tested in two different atmospheres, air and 50% H_2/50% N_2, and at different temperatures in the range from 100°C to 500°C. The study contributed to better understanding of the conducting mechanisms of $Ba_2In_2O_5$ in air and hydrogen-containing atmospheres.
 [DOI: 10.1149/2.022202jes]

Manuscript submitted August 29, 2011; revised manuscript received October 25, 2011. Published December 15, 2011.

Brownmillerite-structured $Ba_2In_2O_5$ and related materials have attracted significant attention because of their electrical properties.[1–9] Undoped and Ce-doped $Ba_2In_2O_5$ are reported to show oxygen ion conductivity in oxygen and nitrogen atmospheres, as well as protonic conductivity in humid air and hydrogen-containing atmosphere, especially at temperatures below 500°C. Hence, these materials have potential for application as proton-conductive electrolytes in intermediate temperature fuel cells and other electrochemical devices. The mechanism for oxygen and proton incorporation in the structure has been suggested in the literature,[4–6,8,10] Oxygen ion and proton conductivity is related to oxygen vacancies in the structure and is believed to be favoured in the grain boundary region.[5,11] Electrical properties of $Ba_2In_2O_5$ and related materials are shown to depend on the type and level of dopant, on preparation procedure and resulting microstructure, and on atmosphere and porosity.[7,8,11] The presence of water in the structure and its loss in the temperature range between 200–300°C, reported for these materials,[11,12] is another factor that affects their electrical properties. An understanding of the electrochemical processes in these materials and the effects of different parameters on their electrical conductivity could help improve the characteristics and applicability of $Ba_2In_2O_5$ and its derivatives in electrochemical devices. Using the ac impedance technique and theory,[13–20] a much better understanding of the electrochemical processes and the behaviour of $Ba_2In_2O_5$ and related materials can be obtained. The analysis of the ac impedance scans in this work was based on the Bauerle model,[13] where ideal ac impedance spectra of a ceramic polycrystalline material appear in a form of three successive semicircles associated to the bulk impedance (in the high frequency range), grain boundary impedance (at intermediate frequencies) and the charge transfer or electrode impedance (at low frequencies). In some cases, not all three semicircles are shown, due to the overlapping of the semicircles or part of the spectra being out of the range of frequencies.

In this work we use ac impedance spectroscopy to investigate the electrical properties of $Ba_2In_2O_5$ and the effect of dopant (Ce), atmosphere, temperature, grain size and porosity on these properties. Although $Ba_2In_2O_5$ is a well investigated material, a detailed study of this kind has not been reported before.

Experimental

Powder samples of brownmillerite-structured $Ba_2In_2O_5$ (BIO) and $Ba_2In_{1.5}Ce_{0.5}O_{5.25}$ (BIC) were synthesized via two different methods in order to obtain testing samples with different grain sizes – the glycine-nitrate combustion process (GNP) and the solid-state reaction (SS). Jankovic et al.[10] give the detailed preparation process and characterisation of the powders. Powder samples prepared by both techniques were investigated by X-ray powder diffraction at room temperature on a Bruker AXS D8 X-ray diffractometer with a CuKα source. Pellets for ac impedance measurement were prepared from powders made by the GNP process or the solid-state reaction by pressing under 150 MPa in a 20 mm die using a pneumatic press. Powders made by the GNP process had to be calcined to 1300°C for 6 h before pressing and sintering to achieve acceptable morphology for easier handling and sintering. The pressed pellets were sintered at 1350°C for 6 h in the case of the GNP powders and at 1400°C for 6 hours in the case of the SS powders. Composition of the prepared samples was confirmed by X-ray powder diffraction. The resulting grain size of the sintered samples was determined based on the peak broadening in the X-ray scans, using the Scherrer equation. The density of the sintered pellets was determined by the Archimedes principle in ethanol (94–96%, Alfa Aesar, $\rho 20°C = 0.7893$ g/cm^3). Samples for the porosity study were prepared by mixing the BIO and BIC powder samples with pore-former graphite flakes 7–10 μm (Alfa Aesar) before sintering. A short study was performed to determine the amount of the pore-former needed to achieve a desired porosity of the samples. Samples with porosities of 20%, 30%, 40% and 50% were prepared and used for the study. The microstructures of the sintered samples were observed using an Hitachi S-3500N scanning electron microscope (SEM). Platinum paste (Alfa Aesar) was applied on both sides of the sample pellets to act as electrodes and heated to 800°C for 1 h to decompose all binders in the paste.

The ac impedance spectroscopy was performed by using an impedance analyzer IM6 by Zahner Electrinks, with a frequency range between 100 mHz to 8 MHz and an amplitude of 50 mV in a temperature range from 100°C to 500°C. Two different atmospheres were employed, namely dry air (supplied from the atmosphere and dried to contain up to 15 ppm) and a dry hydrogen/nitrogen mixture (50% H_2/50%N_2) for all samples. Nitrogen and hydrogen used in the experiments (Praxair) contained a maximum of 3 ppm (vol) of water and a maximum of 3 ppm oxygen (in N_2) and 1 ppm of oxygen (in H_2). Samples were held at each temperature for 3 h to achieve equilibrium (it was determined experimentally that up to three hours was the time needed for all samples, measured in both atmospheres and at all testing temperatures to stabilize and achieve equilibrium), and impedance measurements were performed every 30 minutes over the three hours. The samples were exposed to the same atmosphere on both sides with a flow rate of 100 sccm. The

* Electrochemical Society Student Member.
** Electrochemical Society Active Member.
z E-mail: dwilkinson@chbe.ubc.ca; jjankovic@chbe.ubc.ca

temperature and gas flow rate were programmed using an AMEL 7902 test setup.

Initially, several tests were performed to determine what part of the impedance spectra was associated with the material resistivity, and what part with the electrolyte/electrode charge transfer. In order to determine the part of the impedance spectra associated with the electrode charge transfer, samples with the same characteristics (composition, porosity, grain size, thickness) were prepared and different electrodes were applied. For testing in air, one set of electrode samples was prepared with the Pt paste, and the other set of electrode samples with Au sputtered by a Polaron Sputter Coater SC7640. In the hydrogen-containing atmosphere, Au electrodes did not perform well so two different Pt paste electrodes were used: in one case Pt paste was applied and heated to 800°C for 1 h, as in the previous study, while in the other case the Pt paste was only dried in the oven to 80°C. In the later case, the electrode was still active but its activity was expected to be somewhat affected by the microstructure and additives in the Pt paste mixture that did not fully decompose at such a low temperature. Different electrodes are expected to result in different sizes of the semicircles associated with the electrolyte/electrode interface impedance, while semicircles associated with the material contribution should remain unaffected. Knowing that, total contribution from the material (R_{b+gb}) itself (bulk and grain boundary) can be determined. Additional separation of bulk (R_b) and grain boundary (R_{gb}) contribution is useful, but very often challenging, due to common overlapping of the ac impedance semicircles associated with these processes. These tests were done for both BIO and BIC samples prepared by the GNP and the solid-state reaction in air and 50% H_2/50%N_2 atmosphere in the temperature range from 100°C to 500°C.

After sample preparation and the preliminary tests described above, a number of ac impedance tests were performed to investigate the effect of different parameters on the ac impedance scans and electrochemical behaviour of the tested samples. The effect of porosity was determined by testing BIO and BIC samples with a range of porosity. The effect of dopant was investigated by comparing the results of undoped $Ba_2In_2O_5$ samples to Ce-doped $Ba_2In_2O_5$ samples. The effect of grain size for both BIO and BIC samples was studied by comparing the samples made by the GNP method, which resulted in a smaller grain size, with the samples made by the solid-state process, which resulted in a larger grain size. And finally, in all studies the samples were tested in two different atmospheres, air and 50% H_2/50% N_2, and at different temperatures in the range from 100°C to 500°C. Ac impedance scans were fitted to an equivalent circuit and the R and C (or λ) parameters determined.

During the testing in 50% H_2/50% N_2 at 300°C and above, BIO-GNP samples showed inductive contribution in the ac impedance scans due to the parasitic inductance of the external wiring of the testing setup.[21] It is important to correct the measured data for the contribution of the inductance, as it can affect the result for the sample resistance. This can be done by calibrating the cell by shorting and subtracting the cell inductance contribution from the actual test data. Data represented by squares in Fig. 1 are the actual measured data with the inductive tail in the high frequency range. Data represented by circles show the corrected data. This correction was applied to all ac impedance scans that demonstrated inductive behaviour.

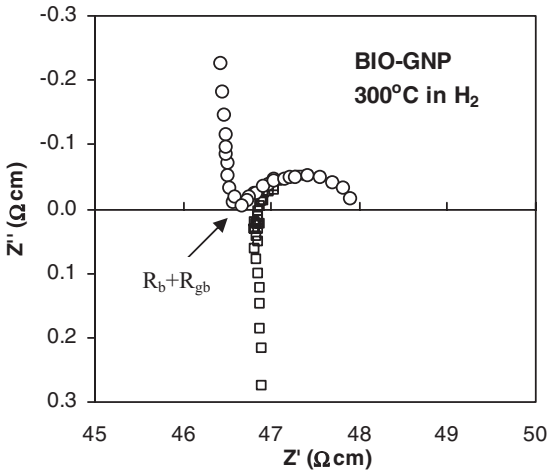

Figure 1. Ac impedance of $Ba_2In_2O_5$ in 50% H_2/50% N_2 at 300°C – correction for the inductance of the external wiring; □ measured data; ○ data corrected for the inductance.

Results and Discussion

Microstructure characterization.— Brownmillerite structured $Ba_2In_2O_5$ and Ce-doped $Ba_2In_2O_5$ powders were produced by both the glycine-nitrate and the solid-state method, as confirmed by X-ray powder diffraction. Fine powders were obtained by the GNP process with an average particle size of about 160 nm and an initial grain size about 10 nm, while the SS process produced coarser powders with an average particle size of about 1.5 μm and a grain size of about 40 nm. These powders were used to prepare sintered samples for the conductivity measurements. Characteristics of the sintered samples used in the ac impedance measurement studies are given in Table I. Grain size of the sintered samples was determined from the X-ray scans using the Scherrer formula, and porosity determined by the Archimedes principle. Fully dense sintered pellet samples could not be prepared due to the limitation of the sintering temperature (above 1400°C the structure of the materials changes to cubic[10]). The lowest porosity obtained without the use of the pore-former was between 16 and 20%. All samples for the ac impedance spectra were produced with a total porosity of about 20% in order to minimize the effect of the porosity factor on the conductivity results. They all had brownmillerite structure as the final phase. Sintered pellet samples produced from the GNP powders had a final grain size of about 40 nm, while the pellet samples made from the solid-state powders had a grain size around 60 nm. In the study to determine effect of the porosity of BIO–GNP and BIC-GNP samples on the conductivity, additional samples with the porosities of 30%, 40% and 50% were prepared. They all had similar grain size, as shown in Table I. Fig. 2 shows SEM pictures of the top-view of a BIO sample made by the solid-state reaction (BIO-SS), a BIO sample made by the GNP reaction (BIO-GNP) and a BIC sample made by the GNP reaction (BIC-GNP). While BIO and BIC samples made by the GNP process have comparable microstructures, the solid-state sample shows a much coarser microstructure.

Determination of electrode contribution.— In order to distinguish the contribution of the sample/electrode interface impedance from the desired material impedance, samples with different electrode materials (Au and Pt) were tested by ac impedance spectroscopy and their scans compared. Fig. 3 shows an example of the ac impedance spectra measured in air at 300°C for BIO and BIC samples made by the GNP process and comparison between the scans obtained when two different electrodes were used. The difference in the low frequency

Table I. Summary of properties and sintering temperatures for pellets used in ac impedance measurements. All compositions have the brownmillerite structure.

Sintered sample (compos.-method)	Sintering T (6h) (°C)	Grain size (nm)	Porosity (%)
BIO-GNP	1350	42	18
BIO-SS	1400	57	20
BIC-GNP	1350	42	20
BIC-SS	1400	60	21
BIO-GNP - 30	1350	40	32
BIO-GNP - 40	1350	42	41
BIO-GNP - 50	1350	41	51

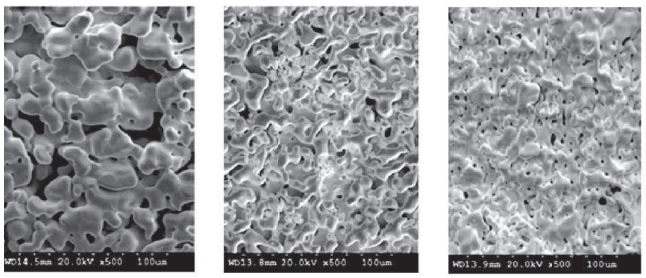

Figure 2. SEM images of three different samples (20% porosity): (1) BIO sample produced by the solid-state reaction, pressed and sintered to 1400°C for 6 h; (2) BIO sample produced by the glycine-nitrate method and sintered to 1350°C for 6 h; (3) BIC sample produced by the glycine-nitrate method and sintered to 1350°C for 6 h.

semicircles is evident for both cases, confirming that this semicircle is due to the electrode contribution. High frequency semicircles are similar (one in the case of BIO and two in the case of BIC) showing that they represent the material contribution. The results are in agreement with the expected behaviour based on the literature.[13,22] where ac impedance spectra of a ceramic polycrystalline material appears in a form of three successive semicircles associated to the bulk impedance (in the high frequency range), grain boundary impedance (at intermediate frequencies) and the charge transfer or electrode impedance (at low frequencies). In some cases, not all three semicircles are shown. Arrows in Fig. 3 show the places where the electrode semicircle starts. The same method was done for BIO and BIC samples prepared by the solid-state method, as well as the GNP method, in both air and hydrogen-containing atmospheres and for each temperature of interest.

Effect of porosity on conductivity.— BIO-GNP and BIC-GNP samples were used for this study, in both air and 50% H_2/50% N_2. The samples were dried at 380°C for 3 h before measurement to release the water. Investigation of different porosities between 20% and 50% showed that the conductivities of the samples decreased with an increase in porosity. Fig. 4. shows an example of the change in the ac impedance scans with the porosity, measured in air at 400°C for the BIO and BIC samples. BIC sample clearly shows the change in the second semicircle with the change of porosity, while the bulk semicircle is unaffected. This is expected, as the bulk impedance does not depend on the geometry and microstructure of the sample. Second semicircle is, therefore, associated not only to the grain boundary resistance, but also to the microstructure of the sample. For the BIO sample, bulk and grain boundary semicircles could not be resolved, and the effect of porosity is shown as an increase of the shown semicircle. Fig. 5. shows the change of the conductivity with the porosity for the BIO and BIC samples measured in air and in hydrogen-containing atmospheres. As similar trends were found in hydrogen atmosphere, only data at one temperature are shown.

Effect of grain size - BIO-GNP and BIO-SS in air.— Fig. 6 shows ac impedance scans for the BIO samples measured in air in the temperature range from 100°C to 500°C. Results for the samples made by both the glycine-nitrate process (GNP – representing samples with a smaller grain size) and by the solid-state reaction (SS – representing samples with a larger grain size) are shown to determine the effect of grain size. One semicircle appears in the high frequency range for each impedance scan, representing the contribution from the material impedance, while the low frequency tail is part of the electrode contribution, as determined earlier. Bulk and grain boundary semicircles cannot be resolved, as they most likely have similar time constants. When comparing samples with the different grain sizes, it is apparent that the samples with larger grains, and hence smaller grain boundary area (SS samples) show higher impedance. Since bulk impedance is an intrinsic property of the material and does not depend on the microstructure, this higher impedance for the SS samples is due to the grain boundary impedance. Hence, it can be concluded that the grain boundary plays a role in the conductivity of BIO in air (mainly oxygen ion and hole conduction[4,9]), showing higher impedance when the grain boundary area is smaller. The difference in impedance is less apparent at higher temperatures, most likely due to the higher mobility of the oxygen ion and improved conduction both in the in the grain boundaries and in the bulk of the material.

The impedance scans for this case can be modelled using an equivalent circuit with a series of RC elements, which represent bulk, grain

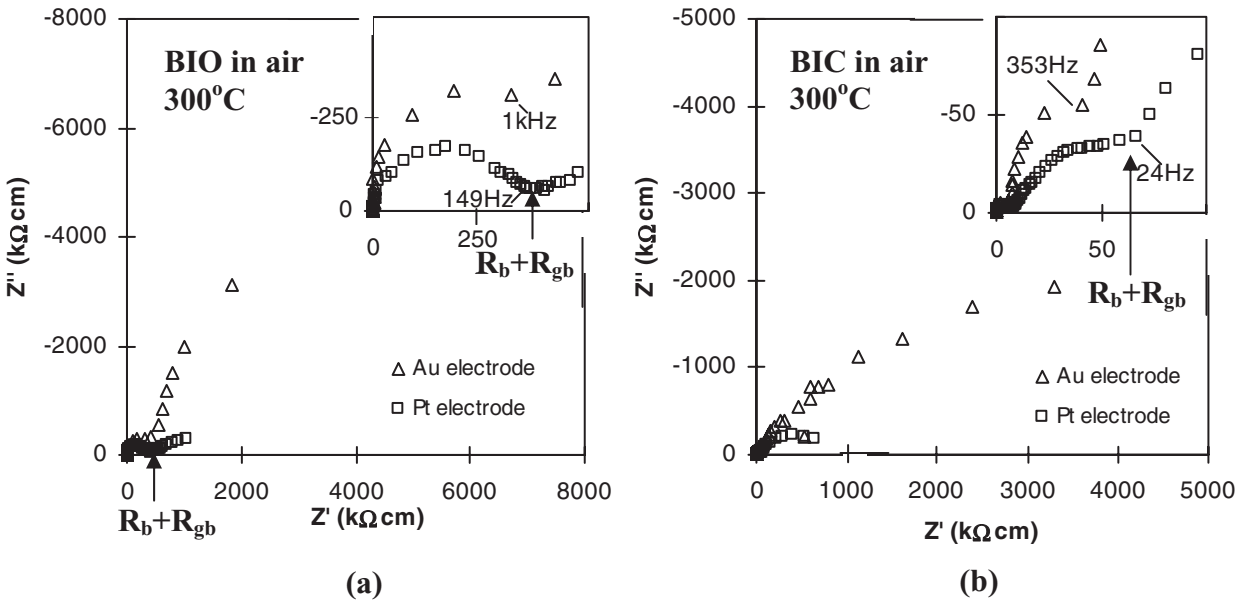

Figure 3. Ac impedance scans measured in air showing the difference between the sample/electrode interface contribution when two different electrodes are applied (Au and Pt); (a) BIO sample made by the GNP process; (b) BIC sample made by the GNP process; Frequencies are given for the points where the material contribution semicircle transitions to the electrode semicircle.

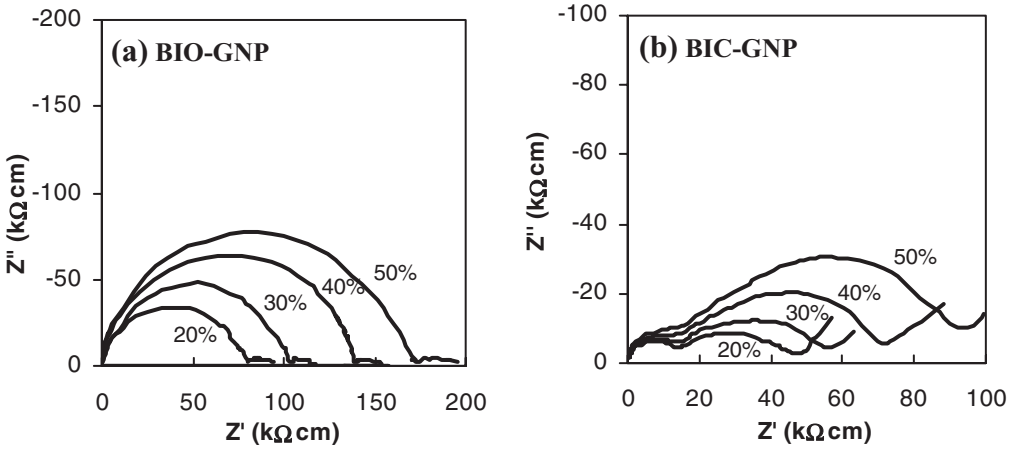

Figure 4. Change in ac impedance scans with porosity for BIO-GNP (a) and BIC-GNP (b) samples measured in air at 400°C (samples were dried before measurement to release water).

boundary and electrode impedance. In a more general case, the scans can be modelled using constant phase elements, $Z(CPE) = \lambda/(j\omega)^{\alpha}$,[13] in combination with R elements, considering RC elements a special case when $\lambda = C$, and $\alpha = 1$. The equivalent circuit used for fitting the impedance plots is shown in Fig. 7. Determined values for R, λ (or C in the case of $\alpha = 1$) and α are shown in Table II for both SS and GNP BIO samples. Since the bulk and grain boundary semicircles could not be resolved, the total value of the material resistance is shown. The values for α are all equal 1, showing that material impedance can be represented as a simple RC element. While the total resistances are decreasing with the temperature, the capacitances are generally increasing.

During the measurement in air, conductivity starts decreasing as a function of time for both GNP and SS samples at 300°C and eventually stabilizes after about 3 hours. This effect is shown in Fig. 8 for the SS sample. This behaviour is due to the loss of water from the structure around 300°C that is reported in our earlier work[10] and by Hashimoto et al.[11] As reported by Zhang et al.[3] water in $Ba_2In_2O_5$ provides protonic conductivity, significantly contributing to the total conductivity measured in air. As the water leaves the structure, the conductivity decreases until it reaches a stable value, when most of the water has left the structure.

Effect of dopant - BIC-GNP and BIC-SS in air.— Fig. 9. shows the ac impedance scans as a function of temperature measured in air for the Ce-doped $Ba_2In_2O_5$, denoted as BIC in this work. The effect of dopant on conductivity of the oxide materials is often related to the segregation of the dopant in the grain boundary region.[21,23,24] It can be also due to a different symmetry, lattice distances, charge accumulation, concentration of oxygen vacancies, etc. From the ac scans it is apparent that the total resistances of BIC in air are lower than the resistances measured for BIO samples. Bulk and grain boundary semicircles could not be resolved at 100°C, but are clearly shown at 200°C and 300°C, especially for the GNP samples. The low frequency tail is related to the electrode contribution as determined earlier. In the scans taken at 200°C and 300°C, the bulk impedance is the same for the SS and the GNP samples, what was expected, as this impedance does not depend on the microstructure. On the other hand, grain boundary

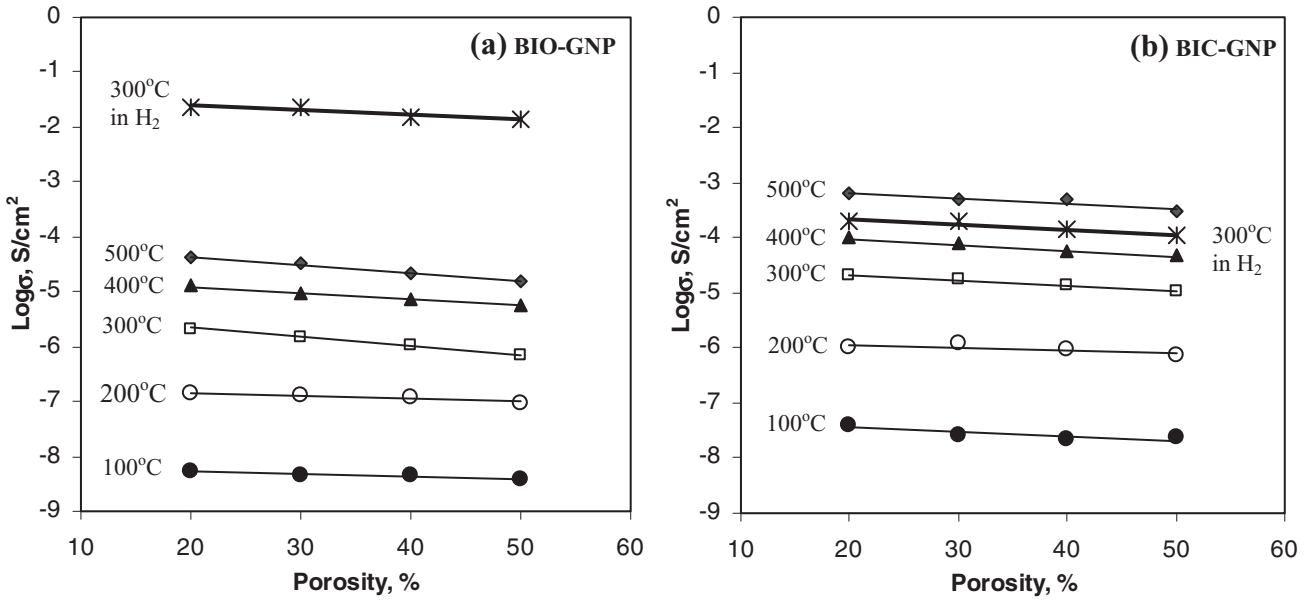

Figure 5. Change in the total electrical conductivity due to different porosities of the BIO-GNP (a) and BIC-GNP (b) samples. Thin lines: data obtained in air. Thick line: example data obtained in 50% H_2/50% N_2 (similar trend obtained at other temperatures).

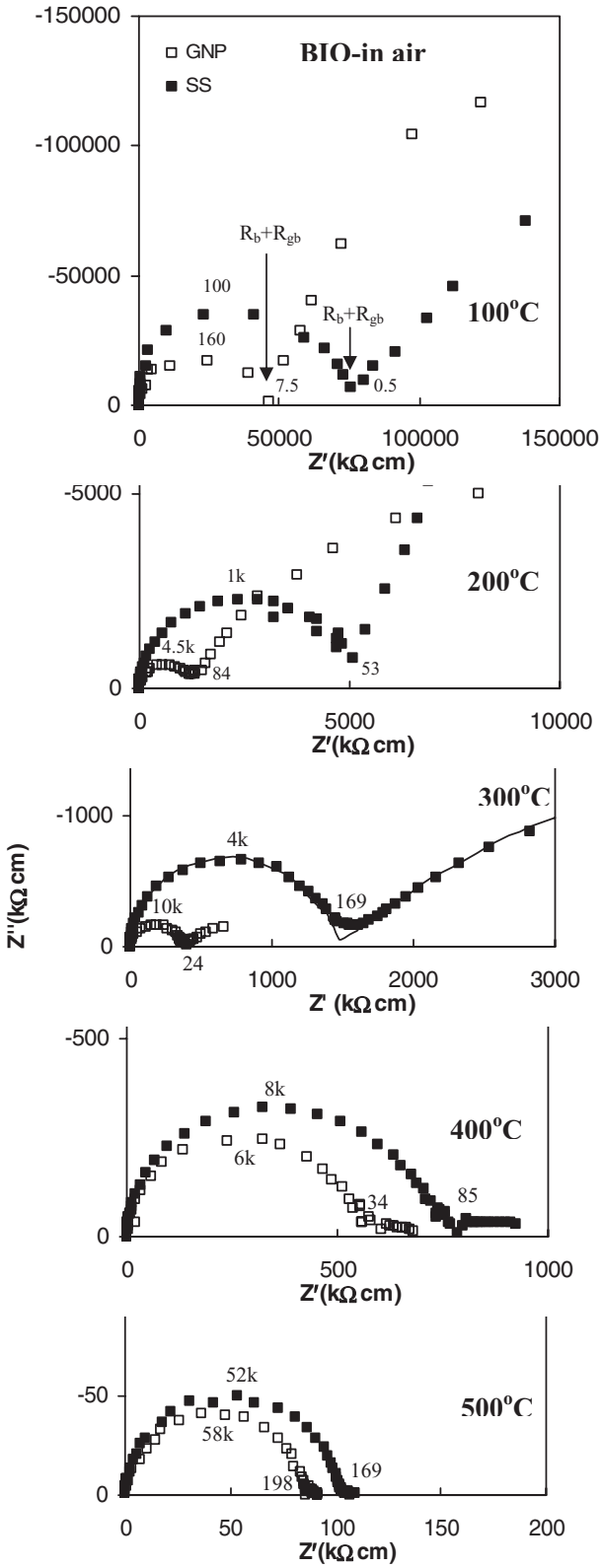

Figure 6. Ac impedance scans for BIO-GNP samples (smaller grain size) and BIO-SS samples (larger grain size) measured in air. Characteristic frequencies are given in Hz. Arrows show the locations where the total material resistance (R_b+R_{gb}) was taken. Line on the 300°C graph shows the equivalent circuit fit to the experimental data.

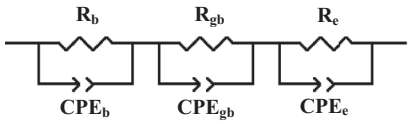

Figure 7. General equivalent circuit used for representing the contribution of bulk, grain boundary and electrode in the total ac impedance response. In a more specific case (when $\alpha = 1$) instead of a CPE, a capacitor C can be used.

impedance is greater for the GNP samples, compared to the SS samples. This result reveals that BIC shows a significant grain boundary resistance to the charge carriers in air, and the larger grain boundary area (for the GNP samples) causes higher grain boundary impedance. This is opposite to what was noticed for the undoped $Ba_2In_2O_5$ (BIO) and hence shows that presence of Ce affects the conductivity of grain boundaries in $Ba_2In_2O_5$, most likely by segregating in this area and affecting the concentration of oxygen vacancies. This would have to be confirmed with a detailed crystal structure comparison to determine the oxygen vacancy, concentration and local effect of Ce as a dopant. However, the total conductivity is still improved in BIC compared to BIO.

The grain boundary impedance for the GNP samples is greater than the bulk impedance at 200°C, but decreases and approaches bulk impedance at 300°C. For the SS samples, the grain boundary impedance is evidently smaller than the bulk impedance, showing an improvement in conductivity for the samples with larger grains and a smaller grain boundary area. BIC did not show the change in conductivity (or ac scans) due to the water loss, as BIO did, although our previous work[10] showed that BIC released more water than BIO with heating. This suggests that water incorporated in the structure of BIC does not provide significant proton conductivity that contributes to the total conductivity, probably because the water in BIC is mostly bound in the bulk,[10] and proton conduction is mainly occurring in the grain boundary, as will be discussed later.

At 400°C and 500°C, the bulk and grain boundary semicircles are harder to resolve, but there is still some distinction. The scans at 400°C and 500°C show that the total impedance of the GNP samples decreases and becomes smaller than the total impedance of the SS samples. Bulk impedance seems to be different for the GNP and SS samples. A gradual change in scans is noticed at 400°C over time, as shown in Fig. 10. In this figure, the change from the scan after 30 min to scan after 1 h is expected at the equilibration step when the temperature in the test is changed from a lower value to a higher value (300°C to 400°C). However, the further change to the scan after 1.5 h and 2 h is in the opposite direction, towards greater impedances. This change is most likely related to the phase change from a brownmillerite to a cubic structure that is reported to occur in BIC samples above 400°C.[10] This change to the cubic structure causes an increase in bulk and grain boundary impedance.

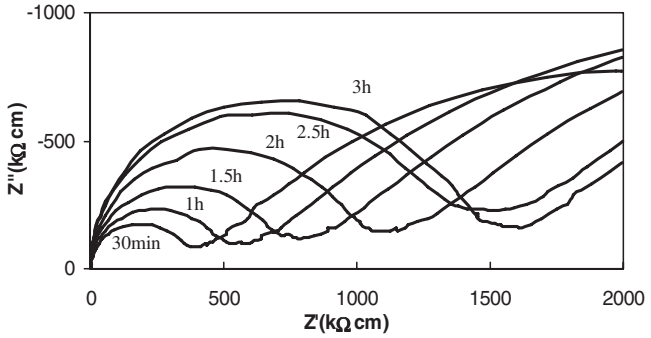

Figure 8. Change in the ac impedance spectra for BIO-SS samples at 300°C over time, due to loss of water. Scans stabilize after about 3 hours.

Table II. BIO sample measured in air – parameters determined by fitting the experimental ac scans to the equivalent circuit shown in Fig. 7.

	SS (grain size ≈ 60 nm)			**GNP** (grain size ≈ 40 nm)		
T, °C	R_{b+gb}, ohm · cm	λ (or C_{b+gb}), F/cm	α	R_{b+gb}, ohm · cm	λ (or C_{b+gb}), F/cm	α
100	7.58E + 07	2.10E-11	1.00	4.63E + 07	2.15E-11	1.00
200	4.80E + 06	3.32E-11	1.00	1.30E + 06	2.72E-11	1.00
300	1.50E + 06	2.54E-11	1.00	3.64E + 05	4.13E-11	1.00
400	7.65E + 05	2.60E-11	1.00	5.46E + 05	4.80E-11	1.00
500	1.02E + 05	3.00E-11	1.00	8.40E + 04	3.27E-11	1.00

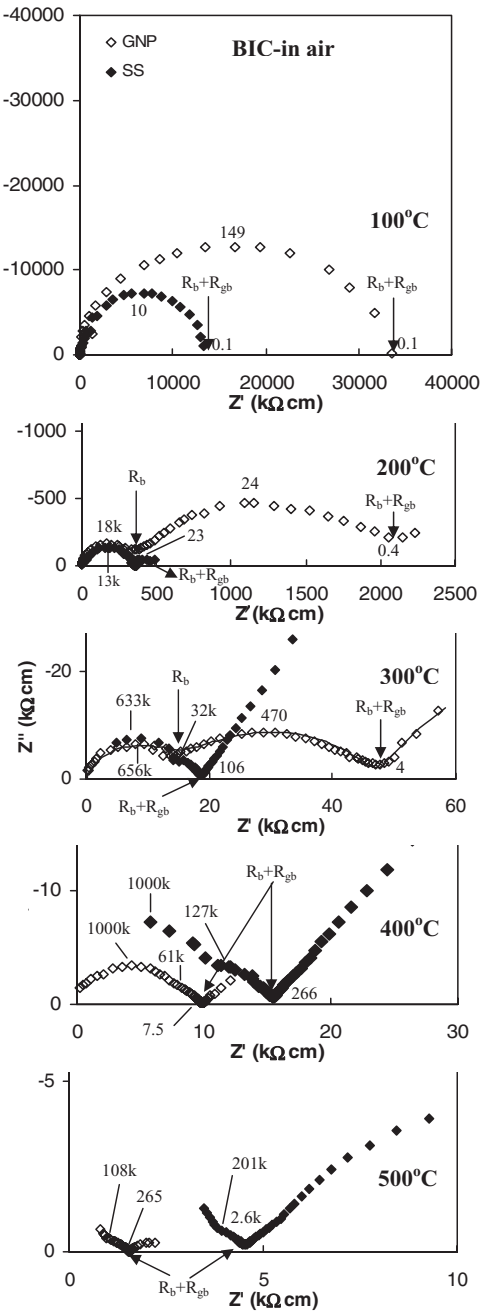

Figure 9. Ac impedance scans for BIC-GNP samples (smaller grain size) and BIC-SS samples (larger grain size) measured in air. Characteristic frequencies are given in Hz. Arrows show the locations where the bulk (Rb) and the total material resistance (R_b+R_{gb}) were taken. Line on the 300°C graph shows the equivalent circuit fit to the experimental data.

The ac impedance results for the BIC samples measured in air were fitted to the equivalent circuit shown in Fig. 9. For this case, bulk and grain boundary semicircles were possible to define and values for R_b, λ_b (or C_b), R_{gb} and λ_{gb} (or C_{gb}) are given in Table III. An example of a fit is given in Fig. 9. It can be seen in the table that the bulk capacitances are somewhat smaller than in the case of BIO. Grain boundary capacitances are about two orders of magnitude higher, resulting in a well defined semicircle in the ac impedance scans. Values for α in the CPE elements are generally close to one for the SS samples, while having lower values for the GNP values, especially for the grain boundary semicircle. This behaviour is expected and often happens in polycrystalline materials due to the anisotropy of the material, which is higher in the grain boundary area.[24]

BIO-GNP and BIO-SS in 50% H_2/50% N_2.— When undoped $Ba_2In_2O_5$ was measured in 50% H_2/50% N_2 atmosphere, one semicircle was present in the ac impedance scan at 100°C, for both the GNP and the SS samples, as shown in Fig. 11. Bulk and grain boundary semicircles could not be resolved, and the electrode contribution is out of the frequency range (lower limit is 0.1 Hz). Total resistivity, taken as the intercept of the semicircle with the real axis, is quite close to the resistivity measured in air. SS samples showed higher total impedance, suggesting greater grain boundary impedance, as the bulk impedance should be the same for the same samples. This is most likely due to the decreased grain boundary area. At 200°C, while GNP samples still show one semicircle with resistivity close to that measured in air, the SS samples start to show two distinguishable semicircles due to the bulk and the grain boundary contribution. The grain boundary seems to contribute much more to the total resistance.

For these SS samples, the grain boundary contribution decreases at 300°C, while bulk resistance becomes predominant. Fig. 12 shows a change over time that occurs at 300°C for the SS samples. The impedance of the sample decreases, especially in the grain boundary area, shown as the decrease in the size of the grain boundary arc. This change is again related to the loss of water at around 300°C. However, the change is opposite to what was seen in air. In this case the total impedance is decreasing and conductivity improving over time. As

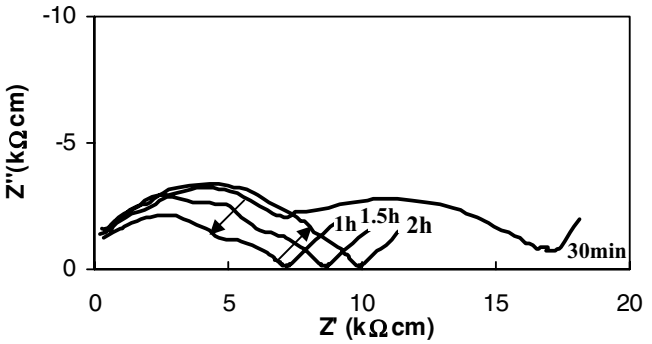

Figure 10. Ac impedance scans measured in air at around 400°C showing the change in impedance for BIC-GNP samples with time due to the phase change. Scans stabilize after 2 hours.

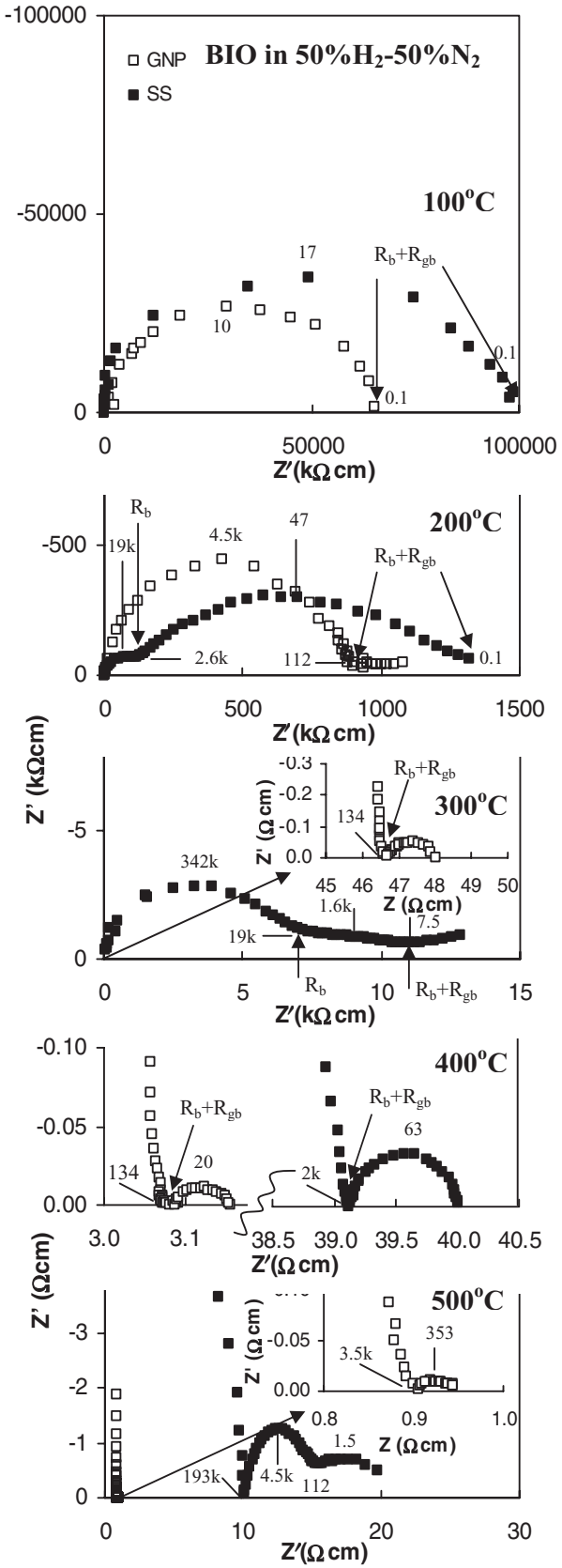

Figure 11. Ac impedance scans for BIO-GNP samples (smaller grain size) and BIO-SS samples (larger grain size) measured in 50% H_2/50% N_2. Characteristic frequencies are given in Hz. Arrows show the locations where the bulk (Rb) and the total material resistance (R_b+R_{gb}) were taken.

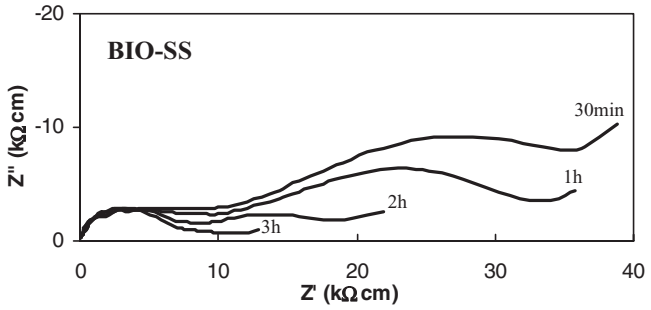

Figure 12. Change in ac impedance scan for BIO-SS samples measured in 50% H_2/50% N_2 atmosphere at 300°C. The change is due to the loss of water and direct incorporation of hydrogen that provides proton conductivity.

suggested in our other work,[8] this is due to the loss of water from the structure and direct hydrogen incorporation into the structure, providing improved protonic conductivity. As it can be seen in the figure, while bulk impedance is not affected by this change, the grain boundary area is significantly affected. This suggests that most of the water is incorporated in the grain boundary region, as also suggested in our earlier work,[10] and that hydrogen also incorporates mostly in that region.

Fig. 11, inset for the scans at 300°C, shows the ac impedance scan for the BIO-GNP samples. A radical decrease in resistivity at 300°C and a change in the ac impedance scan occur. The total resistance drops from ∼1000 kΩcm at 200°C to ∼46 Ωcm at 300°C. The low frequency semicircle represents the electrode resistance. The total resistance of the material was taken to be value R_{b+gb} on the graph. This value proportionally changed with the thickness of the samples, which confirmed that R_{b+gb} corresponds to the total resistance of the material. The shown semicircle is associated to the electrode impedance, while the tail in the high frequency range is the beginning of the material impedance semicircle. This as also confirmed in the initial study discussed earlier, where we determined the electrode contribution to ac impedance spectra.

Because of the significant change between the ac scans at 200°C and 300°C for the BIO-GNP samples measured in hydrogen-containing atmosphere, more studies were performed between these two temperatures and at 300°C. The ac impedance scans measured between 200°C and 300°C, as well as over the 3-hour period at 300°C are shown in Fig. 13. Starting at 240°C, Warburg component of the impedance scan appears, revealing a diffusion process that affects the charge transfer. This is again due to the loss of water from the structure. Total impedance of the material is decreasing with the temperature. Warburg component is present up to 290°C. The scan at 290°C has a similar shape as the BIO-SS samples at 300°C (Fig. 11), showing bulk contribution and a depressed grain boundary contribution. The main resistance seems to be in the bulk of the material. The first scan at 300°C after 30 min, shown in Fig. 13 (top), is shown as one semicircle. The change at 300°C over a 3-hour period is shown in Fig.13 (bottom). Impedance continues to decrease, until it reaches a low value of 46 Ωcm. The shape of the scans changes to show a semicircle associated to the electrode impedance, and a high frequency tail that represents the beginning of the material impedance semicircle (not fully shown because it is out of frequency range). This short study confirms that as the water leaves the structure between 240°C and 300°C, resistivity of the sample in the hydrogen-containing atmosphere decreases several orders of magnitude, most likely due to the incorporation of hydrogen in the structure and proton conductivity. Decomposition of the sample is excluded as the reason for this high conductivity, as neither X-ray diffraction nor the Raman spectra of the samples after the testing show change in composition.[8]

Ac impedance scans for both BIO SS and GNP samples at 400°C, shown in Fig. 11, are similar to impedance scans for the GNP sample at 300°C, but with lower values of impedance. SS samples with

Table III. BIC samples measured in air – parameters determined by fitting the experimental ac scans from Fig. 9. to the equivalent circuit shown in Fig. 7. Note: Values at 100°C marked with * represent total resistance ($R_b + R_{gb}$), as bulk and grain boundary semicircles could not be resolved.

	SS (grain size ≈ 60 nm)					
T, °C	R_b, ohm · cm	λ (or C_b), F/cm	α_b	R_{gb}, ohm · cm	λ (or C_{gb}), F/cm	α_{gb}
100	–	–	–	* 1.33E + 07	1.19E-09	1.00
200	3.52E + 05	2.51E-11	0.85	1.08E + 05	6.20E-09	1.00
300	1.35E + 04	1.70E-11	1.00	4.90E + 03	1.01E-09	0.90
400	1.10E + 04	1.45E-11	1.00	2.60E + 03	4.82E-10	1.00
500	3.70E + 03	1.43E-11	1.00	8.00E + 02	9.90E-10	1.00
	GNP (grain size ≈ 40 nm)					
T, °C	R_b, ohm · cm	λ (or C_b), F/cm	α_b	R_{gb}, ohm · cm	λ (or C_{gb}), F/cm	α_{gb}
100	–	–	–	* 3.36E + 07	3.01E-10	0.85
200	3.52E + 05	2.51E-11	0.85	1.69E + 06	3.93E-09	0.70
300	1.35E + 04	1.70E-11	0.82	3.41E + 04	9.90E-09	0.59
400	7.60E + 03	2.10E-12	0.90	2.20E + 03	1.13E-09	0.75
500	1.02E + 03	5.95E-12	1.00	5.00E + 02	2.95E-09	0.90

smaller grain boundary area had ten times higher total resistance, confirming that the grain boundary plays an important role in conduction of protons. At 500°C, for both GNP and SS samples, initial low impedance increased with time and the shape of the ac scans changed, as shown in Fig. 14. When the measurement was continued for 24 h, the impedances continuously increased. X-ray diffraction analysis after conductivity testing showed decomposition of the sample to $BaCO_3$ and elemental indium. Gradual increase in the resistance and appearance of additional contributions to the total resistance is due to the decomposition and formation of the new phases.

Table IV gives the values for resistances and capacitances for BIO samples measured in 50% H_2/50% N_2 determined from fitting the ac impedance scans in Fig. 11 to the equivalent circuit presented in Fig. 7. Scans at lower temperatures showed one or two semicircles with resistances decreasing with temperature. Bulk capacitances had somewhat higher values compared to measurements in air, but still

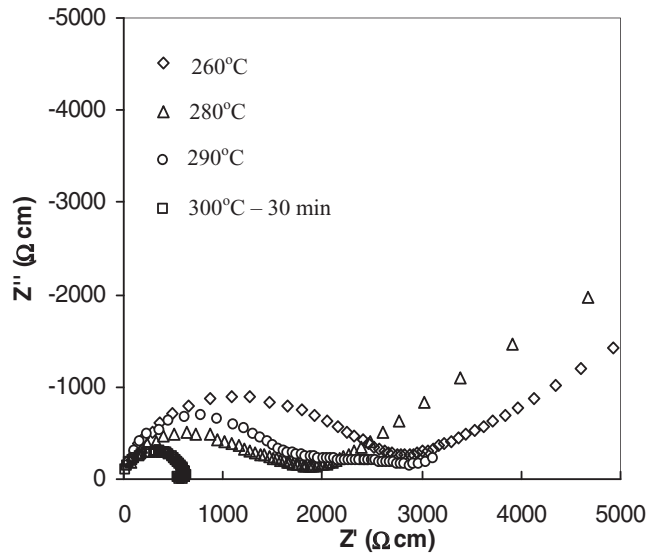

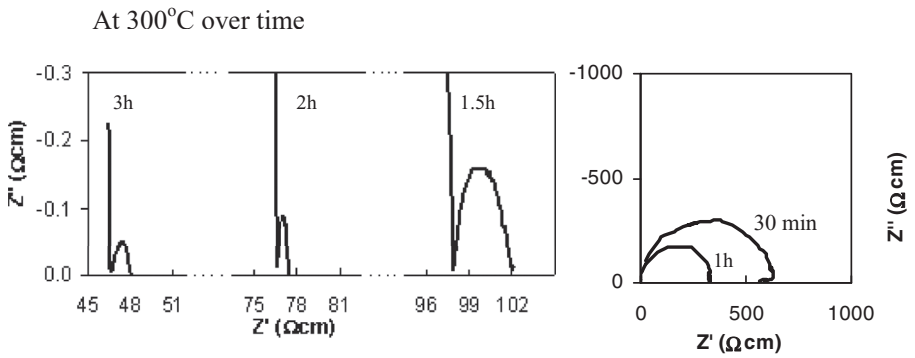

Figure 13. Change in ac impedance scans for BIO-GNP samples in 50% H_2/50% N_2 with loss of water and incorporation of hydrogen between 260°C and 300°C (top) and at 300°C over time.

Table IV. BIO samples measured in 50% H_2/50% N_2 – parameters determined by fitting the experimental ac scan shown in Fig. 11. to the equivalent circuit in Fig. 7. Note: Values marked with * and ** represent total resistance ($R_b + R_{gb}$), as bulk and grain boundary semicircles could not be resolved, where ** marked the cases where full semicircles were not present and therefore values for λ could not be determined.

	SS (grain size≈ 60 nm)					
T, °C	R_b, ohm · cm	λ (or C_b), F/cm	α_b	R_{gb}, ohm · cm	λ (or C_{gb}), F/cm	α_{gb}
100	–	–	–	* 9.74E + 07	9.57E-11	0.80
200	1.19E + 05	7.04E-11	0.90	1.09E + 06	3.11E-09	0.70
300	6.30E + 03	7.39E-11	0.88	2.00E + 03	4.77E-08	0.75
400	–	–	–	** 3.91E + 01	–	–
500	–	–	–	decomp.	–	–
	GNP (grain size≈ 40 nm)					
T, °C	R_b, ohm · cm	λ (or C_b), F/cm	α_b	R_{gb}, ohm · cm	λ (or C_{gb}), F/cm	α_{gb}
100	–	–	–	* 6.54E + 07	2.43E-10	0.88
200	1.19E + 05	7.04E-11	1.00	7.70E + 05	9.00E-11	1.00
300	–	–	–	** 4.67E + 01	–	–
400	–	–	–	** 3.07E + 00	–	–
500	–	–	–	** 9.00E-01	–	–

in the same 10^{-11} F/cm range. Low resistances were achieved at 300°C and higher temperatures in the range between 0.9 Ωcm and 47 Ωcm. Capacitances could not be determined as semicircles were only partially shown, with no defined maximum.

BIC-GNP and BIC-SS in 50% H_2 /50% N_2.— Fig. 15. shows the ac impedance scans measured in 50% H_2/50% N_2 for the Ce-doped $Ba_2In_2O_5$ samples (BIC) made by the GNP and SS method. Effect of Ce-dopant is investigated. At 100°C, for both the GNP and SS samples, one semicircle can be seen, with impedance one order of magnitude lower than when the same samples were measured in air. They are also lower than the impedances in hydrogen-containing atmosphere for BIO samples, showing that Ce as dopant improves the conductivity of $Ba_2In_2O_5$ in hydrogen-containing atmospheres at low temperatures. At 200°C, for both the SS and GNP sample, two semicircles can be distinguished. The semicircle associated to the bulk contribution to the impedance is the same for both samples, as expected, while semicircles due to the grain boundary contribution are larger for the SS samples. This effect is similar to what BIO-SS has shown, suggesting higher resistance in the grain boundary region for the sample with the smaller grain boundary area. Larger grain boundary area enables easier transport of charge carriers. GNP sample even shows that the bulk resistance is predominant in the case when the grain boundary area is large enough. For all other temperatures up to 500°C, similar effects were noticed. At 300°C, while BIO showed a radical decrease in impedance due to water loss and hydrogen incorporation, BIC did not show a significant effect and its impedance continued to linearly decrease. As mentioned before, BIC was shown to contain even larger amount of water in its structure than BIO, and it was expected that BIC shows a stronger effect of water loss. The lack of the same effect could be explained by the hypothesis concluded in our previous work[10] that BIC possibly contains most of the water in the bulk (grain interior), while BIO has it in the grain boundary. If the proton transport is mainly occurring in the grain boundary region at this temperature, as some of our results suggest (Fig. 11, impedance for BIO sample at 300°C and Fig. 15, scan for BIC at 300°C), than water collected in the grain boundary of BIO would affect it, while water collected in the bulk of BIC would have less effect on this transport. This different effect of water in BIO and BIC caused BIC impedance at 300°C to become higher than the impedance of BIO.

At 400°C the impedance of the BIC samples increased (mostly bulk) due to already mentioned phase change from brownmillerite structure to a cubic structure. Grain boundary contribution became negligible for the GNP sample at 400°C and 500°C. Table V gives values for R_b, λ_b (or C_b), R_{gb} and λ_{gb} (or C_{gb}) obtained by fitting the ac impedance scans measured for BIC in 50% H_2/50% N_2 to the equivalent circuit in Fig. 7. Bulk capacitances are somewhat higher than the bulk capacitances for BIC in air, but lower than capacitances

Table V. BIC samples measured in 50% H_2/50% N_2 – parameters determined by fitting the experimental ac scan shown in Fig. 16. to the equivalent circuit in Fig. 6. Note: Values marked with * represent total resistance ($R_b + R_{gb}$), as bulk and grain boundary semicircles could not be resolved.

	SS (grain size≈ 60 nm)					
T, °C	R_b, ohm · cm	λ (or C_b), F/cm	α_b	R_{gb}, ohm · cm	λ (or C_{gb}), F/cm	α_{gb}
100	–	–	–	* 3.06E + 06	5.21E-12	0.95
200	3.90E + 04	2.82E-11	0.82	9.50E + 04	1.68E-09	0.85
300	3.00E + 03	2.12E-11	0.80	1.70E + 04	1.34E-09	0.70
400	6.00E + 03	2.65E-11	0.93	4.00E + 04	8.82E-08	0.55
500	3.10E + 03	2.28E-11	0.93	1.00E + 04	1.00E-06	0.60
	GNP (grain size≈ 40 nm)					
T, °C	R_b, ohm · cm	λ (or C_b), F/cm	α_b	R_{gb}, ohm · cm	λ (or C_{gb}), F/cm	α_{gb}
100	–	–	–	* 9.84E + 05	2.02E-11	1.00
200	3.90E + 04	2.82E-11	0.92	2.50E + 04	5.05E-07	0.55
300	3.00E + 03	2.12E-11	0.90	1.40E + 03	7.58E-07	0.50
400	6.00E + 03	2.65E-11	0.93	6.00E + 02	1.50E-09	1.00
500	3.10E + 03	2.28E-11	0.93	2.00E + 01	9.00E-08	1.00

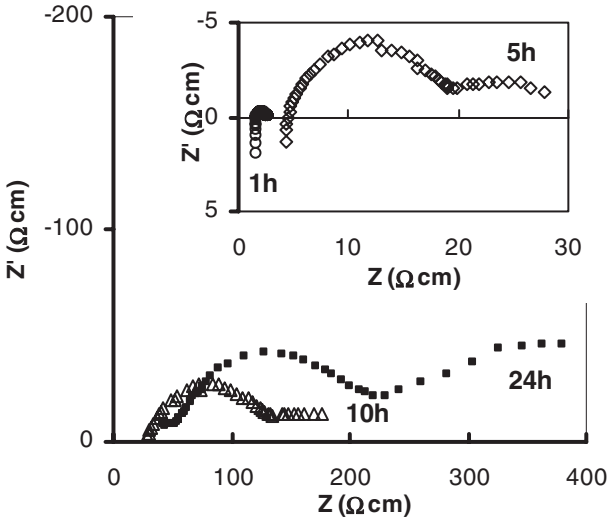

Figure 14. Change of ac impedance scans of $Ba_2In_2O_5$ in 50% H_2/50% N_2 at 500°C with time due to decomposition to $BaCO_3$ and elemental indium.

for BIO in H_2. Grain boundary capacitances are generally higher for BIC in hydrogen-containing atmosphere than in air.

Conductivity comparison.— The total and bulk conductivities of the investigated samples in air and hydrogen-containing atmosphere have been calculated from the impedance data and are shown in Fig. 16.

As it can be seen from Fig. 16a, BIO-GNP has higher conductivity in air than BIO-SS samples due to its larger grain boundary area, as concluded earlier in the ac impedance scan analysis. Bulk conductivity could not be determined for the BIO sample because it could not be separated from the grain boundary contribution in the impedance scans. However, BIC-GNP samples show lower conductivity in air than BIC-SS samples (except at 400°C and 500°C, when the change to a cubic structure occurs), most likely due to the segregation of Ce-dopant in the large grain boundary area and resistance that it causes to the charge transport. Bulk conductivity for the BIC samples is close to the conductivity of the SS samples, suggesting that the main resistance for BIC in air comes from the grain boundary. However, even with this resistance, BIC shows higher total conductivity in air than BIO.

Fig. 16b reveals that BIO-SS and BIO-GNP have similar conductivity in hydrogen at low temperatures. However, as water leaves the structure and hydrogen incorporates at 300°C and above, BIO-GNP shows an order of magnitude higher conductivity. This confirms that hydrogen incorporation and transport is favoured in the grain boundary area. As for the bulk conductivity for the BIO sample, it could be determined only at 200°C and 300°C, while at other temperatures it could not be separated from the bulk contribution in the ac impedance scans. The value at 200°C is an order of magnitude higher than total BIO conductivity, revealing that most of the resistance to the transport of protons from hydrogen is in the grain boundary, due to the presence of water that most likely blocks the sites where protons would otherwise be incorporated. At 300°C, as the water leaves the structure, total conductivity radically increases, with bulk conductivity staying low. This is especially enhanced for the GNP sample, confirming that the process of water release and hydrogen incorporation mainly happens in the grain boundary area. It is interesting to note that BIO bulk conductivity is quite close to the BIC bulk conductivity.

For the BIC samples, BIC-GNP samples showed higher conductivity than BIC-SS samples in hydrogen, revealing that grain boundary plays an important role in charge conduction. Total conductivity of the SS samples is lower than the bulk conductivity, while total conductivity of the GNP sample is similar, showing that smaller grain boundary area causes higher resistance to the charge transport. In general, the

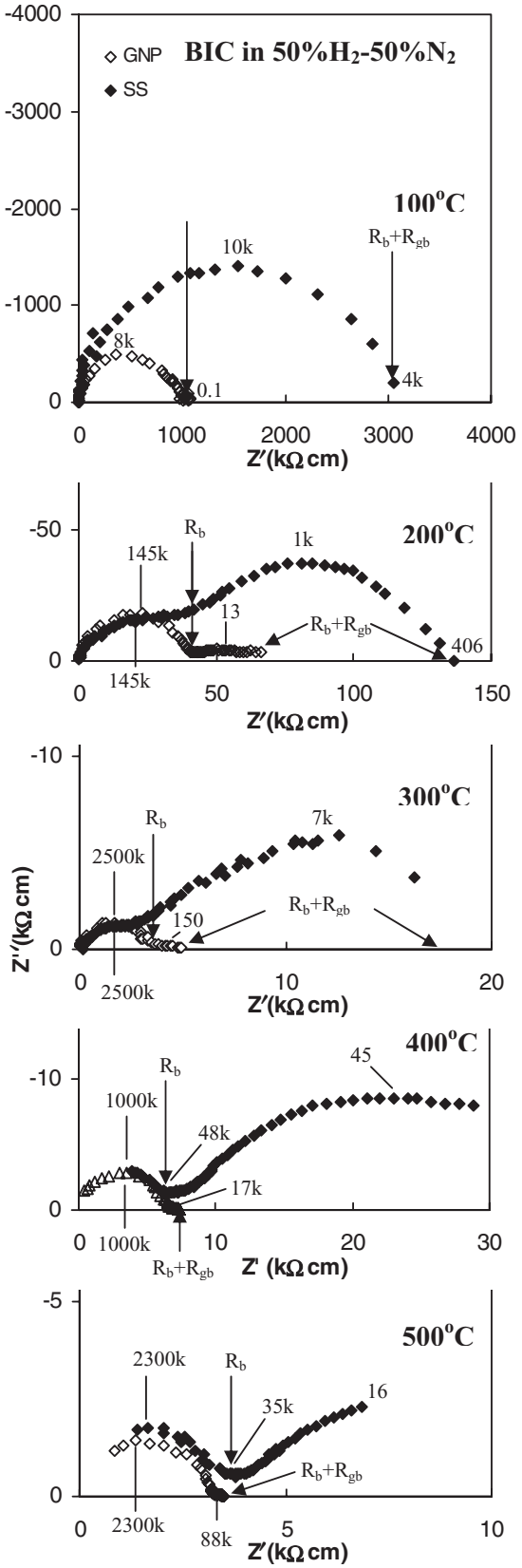

Figure 15. Ac impedance scans for BIC-GNP samples (smaller grain size) and BIC-SS samples (larger grain size) measured in 50% H_2/50% N_2. Characteristic frequencies are given in Hz. Arrows show locations where the bulk (R_b) and the total material resistance (R_b+R_{gb}) was taken.

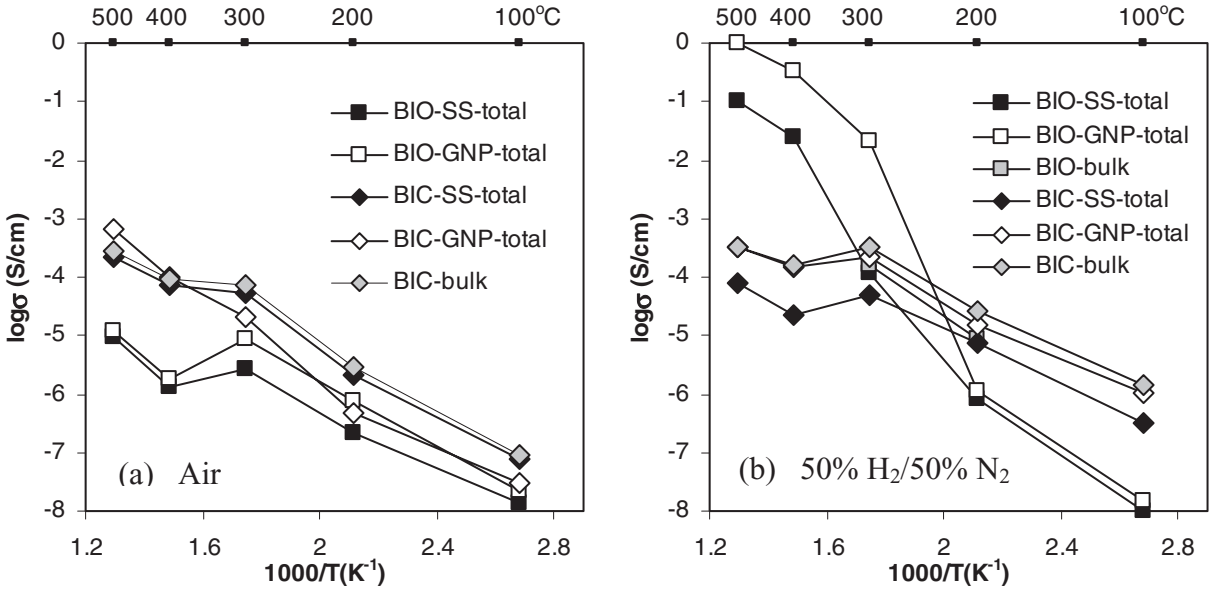

Figure 16. Total and bulk conductivities determined from the ac impedance scans; (a) BIO and BIC samples measured in air; (b) BIO and BIC samples measured in 50% H_2/50% N_2. Note: values for BIC bulk conductivities at 100°C are projected.

effect of microstructure is more enhanced in a hydrogen-containing atmosphere than in air, confirming that the grain boundary area plays a more important role in the charge transport in hydrogen than in air.

Conclusions

Ac impedance spectroscopy was used to investigate electrical properties of $Ba_2In_2O_5$ and Ce-doped $Ba_2In_2O_5$ and the effect microstructure (grain size and porosity), atmosphere, and temperature on its electrical impedance. Sintered sample pellets of brownmillerite-structured undoped $Ba_2In_2O_5$ (BIO) and Ce-doped $Ba_2In_2O_5$ (BIC) were prepared for the study. From the study on the correlation between conductivity and porosity, it was concluded that conductivity decreases with increasing sample porosity and a relationship between porosity and conductivity has been established for the BIO and BIC samples in air and a hydrogen-containing atmosphere. The lowest porosity that could be obtained was in the range of 16 to 20%. Samples with a similar total porosity of 20% were used for the further studies. The solid-state samples (SS) resulted in coarser microstructure and larger grain size (∼60 nm) and the glycine-nitrate samples (GNP) resulted in finer microstructure and smaller grain size (∼40 nm).

Ac impedance scans measured in air between 100°C and 500°C showed only one semicircle for BIO, due to overlapping of bulk and grain boundary semicircles, while BIC showed two distinguished semicircles at most temperatures allowing the bulk and grain boundary impedance to be determined. BIO-SS samples with their larger grains and, hence, smaller grain boundary area resulted in higher total impedance compared to BIO-GNP samples, showing that grain boundary area plays an important role in charge transfer in air, and that larger area favours the charge transport. During the measurement at 300°C BIO samples loose the water bound in their structure and their conductivity drops over time, since water provides some protonic conductivity. While BIC samples did not show a significant effect of water loss at 300°C (conductivity constant over time), it showed a change in scans at 400°C due to the phase transformation from the brownmillerite structure to a cubic structure.

Doping with Ce led to a decrease in total impedance in air and therefore improved conductivity of the material in air. BIC-GNP samples showed that most of the resistance is in the grain boundary area, most likely due to the Ce segregation in this area. The smaller grain boundary area of the SS samples caused lower resistance.

For measurements in hydrogen-containing atmospheres, the total impedance of the BIO SS and GNP samples at 100°C and 200°C was similar to the impedance measured in air, but at higher temperatures a radical decrease in impedance was noticed. Warburg impedance present in the scans between 240°C and 300°C revealed loss of water and the significant decrease in impedance at 300°C was associated with the direct incorporation of hydrogen to provide proton conductivity. The change in the grain boundary semicircle in the ac impedance scans for the BIO-SS samples in that temperature range suggests that the process of water release and hydrogen incorporation mainly occurs in the grain boundary area. The resistivities as low as a few ohms to several tens of ohms were achieved at 300°C and above. It was confirmed that this high conductivity was not related to a chemical decomposition. However, at 500°C and above both GNP and SS samples start to decompose to $BaCO_3$ and elemental In, which was also indicated in the ac impedance scans.

Again in hydrogen-containing atmosphere, Ce-dopant improved conductivity at lower temperatures compared to the BIO sample. However, BIC samples did not show the same radical decrease in impedance due to the release of water and hydrogen incorporation, as BIO did, even though it has been shown in our previous work that BIC contains larger amounts of water in the structure. This is because most of the BIC water is bound in the bulk and its release would not significantly affect the proton conductivity that is mainly occurring in the grain boundary area. The important role of the grain boundary area in the proton conductivity was confirmed by the effect of the microstructure on the grain boundary semicircle of the impedance scan. A larger grain boundary area for GNP samples enables easier transport of protons, and therefore results in a smaller grain boundary impedance semicircle. Also in hydrogen, the BIC samples experienced a change to a cubic structure at 400°C, which caused an increase in impedance, especially the bulk impedance.

All ac impedance scans obtained for BIO and BIC samples in both air and hydrogen-containing atmospheres were fitted to a general equivalent circuit with R and CPE elements and values for the bulk and grain boundary resistances and capacitances were determined. In addition, Arrhenius graphs were constructed from the measured resistance, and conductivity (total and bulk) changes with temperatures for all cases shown. Analysis of the conductivity results confirmed the conclusions from the ac impedance scans.

Acknowledgments

Financial support from the Natural Sciences and Engineering Research Council of Canada (NSERC) for this project is gratefully acknowledged. The authors would also like to thank the National Research Council-Institute for Fuel Cell Innovation (NRC-IFCI) for support of this project.

References

1. T. Norby, *Solid State Ionics*, **125**, 1 (1999).
2. C. A. J. Fisher and M. S. Islam, *Solid State Ionics*, **118**, 355 (1999).
3. G. B. Zhang and D. M. Smyth, *Solid State Ionics*, **82**, 161 (1995).
4. R. Hui, R. Maric, C. Decès-Petit, E. Styles, W. Qua, and X. Zhang et al., *J. Power Sources*, **161**, 40 (2006).
5. N. Bonanos, *Solid State Ionics*, **53–56**, 967 (1992).
6. G. B. Zhang and D. M. Smyth, *Solid State Ionics*, **82**, 153 (1995).
7. J. Niwa, T. Suehiro, K. Kishi, S. Ikeda, and M. Maeda, *J. Mat. Sci.*, **38**, 3791 (2003).
8. J. Jankovic, D. P. Wilkinson, and R. Hui, *J. of Electrochem. Soc.*, **158**(1), B61 (2011).
9. T. Schober and J. Friedrich, *Solid State Ionics*, **113–115**, 369 (1998).
10. J. Jankovic, D. P. Wilkinson, and R. Hui, *J. Power Sources*, (first revision submitted).
11. T. Hashimoto, Y. Inagaki, A. Kishi, and M. Dokiya, *Solid State Ionics*, **128**, 227 (2000).
12. K. D. Kreuer, *Solid State Ionics*, **125**, 285 (1999).
13. J. E. Bauerle, *J. Phys. Chem. Solids*, **30**, 2657 (1969).
14. E. Barsoukov and J. R. Macdonald, *Impedance Spectroscopy – Theory, Experiment, and Applications*, 2nd edition, John Wiley & Sons, Inc. New Jersey (2005).
15. E. V. Ramana, S. V. Suryanarayana, and T. B. Sankaram, *Mater. Res. Bull.*, **41**, 1077 (2006).
16. S. Dutta, R. N. P. Choudhary, and P. K. Sinha, *Eur. Phys. J. Appl. Phys.*, **36**(2), 141 (2006).
17. K. Huang, R. S. Tichy, and J. B. Goodenough, *J. Am. Ceram. Soc.*, **81**[10], 2576 (1998).
18. D. K. Pradhan, B. K. Samantaray, R. N. P. Choudhary, and A. K. Thakur, *J. Mat. Sci.*, **40**, 5419 (2005).
19. T. S. Zhang, J. Ma, Y. Z. Chen, L. H. Luo, L. B. Kong, and S. H. Chan, *Solid State Ionics*, **177**, 1227 (2006).
20. M. J. Verkerk, B. J. Middelhuis, and A. J. Burggraaf, *Solid State Ionics*, **6**, 159 (1982).
21. D. Vladikova, J. A. Kilner, S. J. Skinner, G. Raikova, and Z. Stoynov, *Electrochimica Acta*, **51**, 1611 (2006).
22. H. Duncan and A. Lasia, *Solid State Ionics*, **176**, 1429 (2005).
23. W. Lai and S. M. Haile, *J. Am. Ceram. Soc.*, **88**[11], 2979 (2005).
24. J. R. Macdonald and W. R. Kenan, *Impedance Spectroscopy Emphasizing Solid Materials and Systems*, John Wiley & Sons, New York (1987).